

## High Power Operation of an X-Band Gyrotwistron

P. E. Latham, W. Lawson, V. Irwin, B. Hogan, G. S. Nusinovich, H. W. Matthews, and M. K. E. Flaherty  
*Institute for Plasma Research and Electrical Engineering Department, University of Maryland, College Park, Maryland 20742*  
 (Received 21 October 1993)

We report the first experimental verification of a gyrotwistron amplifier. The device utilized a single 9.858 GHz, TE<sub>011</sub> cavity, a heavily attenuated drift tube, and a long tapered output waveguide section. With a 440 kV, 200–245 A, 1  $\mu$ s electron beam and a sharply tapered axial magnetic field, peak powers above 21 MW were achieved with a gain near 24 dB. Performance was limited by competition from a fundamental TE<sub>11</sub> mode. A multimode code was developed to analyze this system, and simulations were in good agreement with the experiment.

PACS numbers: 85.10.Jz, 41.75.Ht

Devices based on the cyclotron maser instability [1,2] have proven to be efficient, high power, high frequency rf sources (see, e.g., [3]). Oscillator configurations include the gyrotron, which has received the largest effort to date [4–6], and the gyrobackward wave oscillator (gyro-BWO) [7]. Gyrotraveling wave tubes (gyro-TWTs) [8] and gyroklystrons [9–12] have successfully demonstrated high power amplification. Applications for these gyrodevices include plasma heating and current drive, deep space and conventional radar, drivers for rf accelerators and supercolliders, and materials processing. Some of these applications require high efficiency, high power amplifiers. A possible candidate for a source with these requirements is the gyrotwistron.

The gyrotwistron is closely related to the twystron [13], a linear beam device which utilizes the bunching cavities of the klystron with the output waveguide of the TWT. In an analogous fashion, the gyrotwistron utilizes the bunching cavities of the gyroklystron with the output waveguide of the gyro-TWT. In comparison with the gyroklystron, the gyrotwistron has at least one important advantage: it can sustain higher powers. This is because it has significantly better output coupling than the gyroklystron, whose output cavity has a high quality factor. Therefore, for the same amplitude electromagnetic field in the interaction region, the radiated power is significantly higher in the gyrotwistron. Since this field is limited by breakdown, the gyrotwistron is capable of producing higher microwave power than the gyroklystron. The gyrotwistron also has an advantage over gyro-TWTs because its interaction length is shorter. This is important for the suppression of parasitic modes, whose starting current typically scales inversely as the cube of the length.

In spite of these advantages, researchers have not paid close attention to the gyrotwistron. It was examined theoretically in the 1970s [14,15] for weakly relativistic electron beams, and recent work has extended the modeling to the relativistic case [16,17] and to the design of an experimentally feasible, weakly relativistic tube [18]. However, to our knowledge, until now there have been no experimental results.

The goal of our work is to verify the potential capabilities of high power gyrotwistrons. Since susceptibility of these tubes to instabilities in the output waveguide is a critical issue, we developed a nonlinear, multimode, multifrequency code to examine both the stability of parasitic oscillations and the efficiency of the operating mode. We used this code to design a gyrotwistron operating in the TE<sub>01</sub> mode at 9.85 GHz, which produced 21 MW with an efficiency of 22%. The output characteristics and stability properties were in good agreement with theoretical predictions.

We designed the gyrotwistron to be compatible with our gyroklystron test facility [19]. The electron beam was produced by a thermionic double-anode magnetron injection gun [20], which was capable of delivering a 1  $\mu$ s, 440 kV pulse at currents up to 245 A. The guide magnetic field was produced by one cathode coil and seven circuit coils, which allowed optimal tapering of the magnetic field. The input cavity was driven by a 2  $\mu$ s, 100 kW, 9.7–10.0 GHz tunable magnetron. An anechoic chamber was used to measure peak output power and mode purity. Previous comparisons with calorimetry measurements resulted in good agreement with the anechoic chamber measurements [11,12].

A schematic of the gyrotwistron is shown in Fig. 1. The input cavity had a length of 1.73 cm and a radius of 2.81 cm, and was loaded with a thin ring of lossy dielectric to achieve the desired quality factor [21]. The measured resonant frequency was  $9.84 \pm 0.01$  GHz and the quality factor was  $260 \pm 20$ . The drift tube consisted of copper

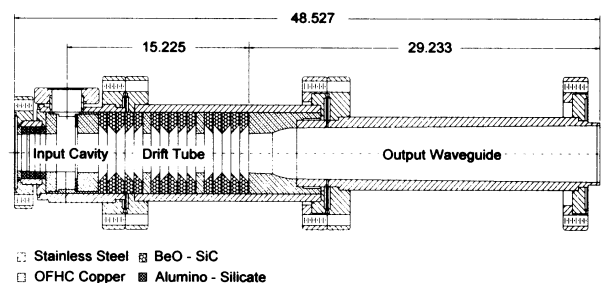


FIG. 1. Tube geometry. Dimensions indicated in cm.

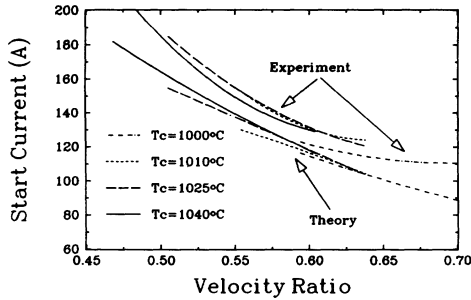


FIG. 2. Experimental measurements and theoretical predictions for the  $TE_{11}$  mode start current. The region above the curves is unstable.

rings alternating with lossy ceramic ones. Attenuation in the  $TE_{11}$  mode (the most troublesome parasite) was greater than 20 dB from 7.0 to 12.0 GHz. The drift tube length was 14.36 cm and the minimum radius was 1.5 cm. The output waveguide section began with a 1.5 cm radius. A 2 cm,  $2^\circ$  taper followed by a 2 cm nonlinear transition brought the wall radius to 1.95 cm. The main section was 25 cm long and had a  $0.5^\circ$  taper to promote stability. A short  $3^\circ$  taper, designed to introduce a slight microwave reflection, ended at a radius of 2.178 cm.

The design of the tube described above proceeded in three steps. The first was to optimize the efficiency of the operating mode using single mode analysis, i.e., ignoring limitations imposed by instabilities. Current and voltage were set at 220 A and 440 kV, respectively (values consistent with our magnetron injection gun), the velocity ratio,  $\alpha \equiv v_\perp/v_\parallel$ , was set to 1, and the velocity spread was determined by an electrostatic gun code [22] to be around 7%. The efficiency was optimized with respect to the magnetic field profile, input power, shape of the output waveguide, and length of the drift section. The second step was to perform a linear analysis to determine the most unstable parasites. We had hoped that the tapered magnetic field and output waveguide would make the parasites linearly stable, but this was not the case. Thus, we had to rely on the operating mode to suppress the parasites nonlinearly, and in the third step we performed simulations using our nonlinear, multimode code. At this step minor modifications were made to the velocity ratio and magnetic field profile to produce a stable design. Details of the formalism used to perform these calculations will be provided in a future publication; here we outline the essential elements of both the linear analysis and the nonlinear, multimode analysis.

To perform the linear analysis for a particular mode, we assumed a steady state, chose a frequency and beam current, and integrated the linearized wave and particle equations through the circuit. At the end of an integration we computed the ratio of the power in the backward wave to the power in the forward wave. This ratio, which we denoted  $R_{eq}$ , is the value of the reflectivity at which the mode is neutrally stable. If the window reflectivity in

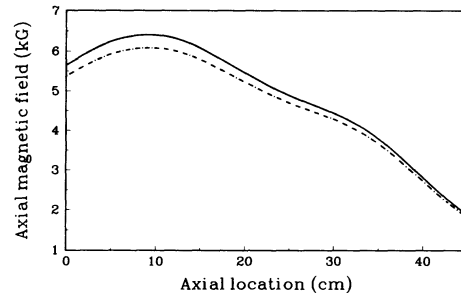


FIG. 3. Axial magnetic field which produced optimum power. Solid line: optimum theoretical field. Dashed line: optimum empirical field.

the experiment,  $R_{window}$ , exceeds  $R_{eq}$ , then the mode is unstable and will grow exponentially in time; otherwise, it is stable and will decay. A mode was considered globally stable if it satisfied  $R_{window} < R_{eq}$  at all currents below the beam current and at all frequencies.

For experimental parameters which yield high efficiency—a beam current near 200 A and a velocity ratio around 1—simulations predicted that a large number of modes were linearly unstable. The worst of these was the  $TE_{11}$  mode at a frequency near 7 GHz, with an equilibrium window reflectivity below 5%. The experimental window reflectivity was much larger, near 50%, which indicates that the  $TE_{11}$  mode should be unstable at a current much less than 200 A and/or a velocity ratio much less than 1. This prediction is consistent with the experiment, in which the most troublesome mode was the  $TE_{11}$  in the 7.0–7.8 GHz range. The start current for this mode, i.e., the current above which it oscillates, is shown in Fig. 2 as a function of velocity ratio for the case when no drive signal is present. Both experimental and theoretical curves are shown. The values of the average velocity ratio were computed from an electrostatic gun code, and the magnetic field profile was the one which yielded the optimum efficiency (see Fig. 3). Agreement between theory and experiment is good, considering the experimental uncertainties in velocity ratio and spread.

Figure 2 indicates that high current can be achieved only at velocity ratios below about 0.5. To achieve high efficiency, however, a velocity ratio near 1.0 with a current of at least 200 A is required. At these values the  $TE_{11}$  mode would be extremely linearly unstable. If the gyrotwistor is to reach high efficiency, the  $TE_{11}$  mode must be suppressed by the operating mode. To calculate the degree of suppression requires a nonlinear, multifrequency, multimode formalism, which we have developed. Briefly this formalism consists of equations for the electrons in the presence of two modes—the operating mode and a parasite—combined with a wave equation for each. We consider steady state operation, so each wave equation is identical in form to the one that would be derived in a single mode theory. Coupling between the two modes is solely through the particles. To simplify the analysis,

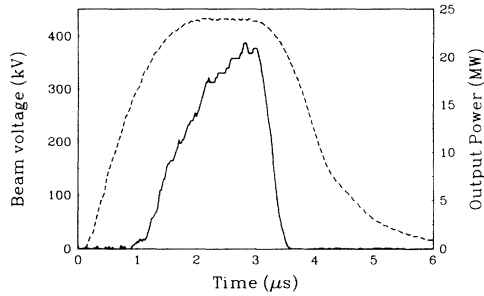


FIG. 4. Time evolution of the amplified signal at the optimal parameters. Solid line: microwave pulse from the X-band detector. Dashed line: voltage pulse.

we average the equations over a cyclotron orbit, ignore space charge, and ignore the effect of the electromagnetic waves on the guiding center radius. To benchmark the code we compared it to the linear code described above, to analytic linear calculations in which the magnetic field and wall radius were held constant, and to a simplified code that included only a single mode. In all cases we found agreement in the appropriate limits. Comparison with experiment, which we discuss below, also provided evidence that our code correctly computes both stability and efficiency.

Experimentally, the search for the optimal operating point proceeded in much the same way as the theoretical one, except slightly different parameters were varied. Since the shape of the output waveguide and the length of the drift section were fixed, the parameters that were varied were the beam voltage and current, drive frequency, magnetic field profile, and beam velocity ratio; the last one via magnetic compression. At a given point in parameter space, we searched for peak power by decreasing the cathode magnetic field (thereby increasing  $\alpha$ ) to a point just before the onset of an instability that degraded the amplified signal. The tube reached its peak power, 21.6 MW, at a voltage of 430 kV and a current of 224 A. The optimal axial magnetic field profile is indicated in Fig. 3. The center of the input cavity is located at  $z = 0$  and the plot extends to the end of the output waveguide section. As shown in Fig. 3, the empirically determined profile was quite close to the optimal theoretical profile.

The peak power results are shown in Figs. 4 and 5. Figure 4 shows the time evolution of the amplified signal at the optimal parameters. The solid line indicates the microwave pulse from the X-band detector; the dashed line represents the voltage pulse. Figure 5 shows the peak power measurement (solid line) and efficiency (dashed line) as a function of beam current. Also shown are the theoretical predictions from numerical simulations.

The peak power and efficiency shown in Fig. 4 were limited by a parasitic  $TE_{11}$  mode. Such competition was also observed in experiments with gyro-TWTs [23], where at high enough drive power single mode operation was observed, while at low power the operating mode was not able to suppress the parasite. Identical behavior occurs

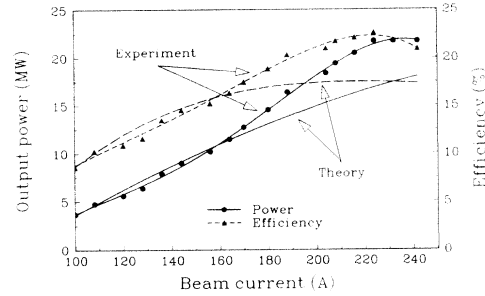


FIG. 5. Peak power (solid line) and efficiency (dashed line) versus beam current, including theoretical predictions. Other parameters are fixed at the optimal values.

in a gyrotwistron: single mode operation at high drive power, coexistence of the operating mode, and a parasite at low drive power. Between these two regimes, several scenarios are *a priori* possible in gyrotwistrons. Simulations of this experiment suggest the one illustrated in Fig. 6. In this figure the efficiency of the operating mode in the presence of the parasite is plotted versus drive power in the first cavity. The dashed line is the operating mode efficiency without the parasite, the solid line is efficiency when the parasite is taken into account. In region III of Fig. 6, the drive power is high enough that single mode operation is the only stable state. In region I, the drive power is so low that the operating mode cannot suppress the parasite and the operating mode and parasite coexist. In region II, there are two possible final states: single mode operation (dashed curve) and multimode operation (solid curve). Which final state the system chooses depends on the initial conditions, and in a device with a long enough pulse that the drive power could be varied, hysteresis could be observed as shown by the arrows in region II.

Figure 6 represents a scenario which can be interpreted not only in terms of the input power but also in terms of the velocity ratio. Two things happen to the curve shown in Fig. 6 as the velocity ratio increases: the peak

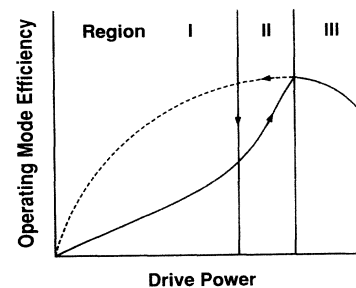


FIG. 6. Cartoon showing how efficiency of the operating mode depends on drive power in the presence of the parasite. Solid (dashed) line is the operating mode efficiency with (without) the parasite. Region I: parasite and operating mode coexist. Region II: both single mode and multimode operation are possible. Hysteresis loop as drive power is varied shown by the arrows. Region III: single mode operation.

efficiency increases, and the transition region, region II, moves to the right, toward higher power. The movement of the transition region to the right occurs because the starting current of parasites decreases as the velocity ratio increases. In an experiment in which the drive power is limited to some finite value, we should observe the following: The efficiency would at first rise with  $\alpha$ , and would continue to rise as long as the peak efficiency remains in region III (the stable, single mode regime) and there is enough drive power to access this region. At high enough  $\alpha$ , the system would switch from region III to region II. Since in our device the initial amplitude of the parasitic TE<sub>11</sub> mode is at the noise level, while the amplitude of the operating TE<sub>01</sub> mode is determined by the input signal and is much larger, it is likely that the single mode state would be accessed in region II as well. However, when the system moves into region I where no single mode state is possible, the operating mode and parasite would coexist. Accompanying this should be a sudden drop in efficiency. This sudden drop in efficiency was observed experimentally, which provides additional evidence for the validity of our analysis.

The theoretical curves in Fig. 5 were made in a manner that parallels the above discussion: efficiency was computed versus velocity ratio at fixed maximum drive power. Voltage and magnetic field profile were those of the experiment, and the axial velocity spread was that predicted by the gun code (about 7% at 224 A, decreasing approximately linearly to 4% at 100 A). The peak efficiency, which occurred just before the system crossed over into region I, is plotted in Fig. 5 versus beam current. Agreement is excellent below 160 A, and good above it.

In summary, peak powers in excess of 21 MW were produced in the first experimental operation of a gyrotwistron. The corresponding efficiency and gain were 22% and 24 dB, respectively. Detailed multimode, multi-frequency comparison with theory was made, and agreement was good. Performance was limited by a TE<sub>11</sub> mode which appeared to be enhanced by window reflections.

Scaling this device to output power levels consistent with the requirements of future linear colliders, such as the Next Linear Collider [24] (100–300 MW in the 10–20 GHz range), is reasonably straightforward. The primary requirements for achieving such power levels are a magnetron injection gun capable of producing a multi-hundred MW electron beam (the beam power in this experiment was slightly less than 100 MW) and the construction of a nonresonant output window. Such a magnetron injection gun has been designed [25], and the construction of a broadband output window is difficult but feasible [26]. And, just as important, the close agreement between theory and experiment gives us confidence in our ability to design stable gyrotwistrons at signifi-

cantly higher power than the one described here.

This work was supported by the U.S. Department of Energy.

- 
- [1] J. Schneider, *Phys. Rev. Lett.* **2**, 504 (1959).
  - [2] A. V. Gaponov, *Izv. Vyssh. Uchebn. Zaved. Radiofiz. Sov. Radiophys.* **2**, 836 (1959).
  - [3] *High Power Microwave Sources*, edited by V. L. Granatstein and I. Alexeff (Artech House, Inc., Norwood, MA, 1987).
  - [4] K. E. Kreischer *et al.*, *Phys. Fluids B* **2**, 640 (1990).
  - [5] V. A. Flyagin and G. S. Nusinovich, *Proc. IEEE* **76**, 644 (1988).
  - [6] K. Felch *et al.*, in *Proceedings of the 18th International Conference on Infrared and Millimeter Waves* (University of Essex, Colchester, U.K., 1993), Conference Digest, p. 517.
  - [7] S. Y. Park *et al.*, *IEEE Trans. Plasma Sci.* **18**, 321 (1990).
  - [8] K. R. Chu *et al.*, *IEEE Trans. Electron. Dev.* **37**, 1557 (1990).
  - [9] A. C. McCurdy *et al.*, *Phys. Rev. Lett.* **57**, 2374 (1986).
  - [10] I. I. Antakov *et al.*, in *Proceedings of the 18th International Conference on Infrared and Millimeter Waves* (Ref. [6]), pp. 338 and 466; I. I. Antakov, E. V. Zasypkin, and E. V. Sokolov, *Proc. SPIE* **2104**, 466 (1993).
  - [11] W. Lawson *et al.*, *Phys. Rev. Lett.* **67**, 520 (1991).
  - [12] W. Lawson *et al.*, *Phys. Rev. Lett.* **71**, 456 (1993).
  - [13] A. D. La Rue and R. R. Rupert, *IEDM*, Washington, D.C., October 1964; A. S. Gilmour, Jr., *Microwave Tubes* (Artech House, Inc., Norwood, MA, 1986).
  - [14] V. L. Bratman *et al.*, *Radiophys. Quantum Electron.* **16**, 474 (1973).
  - [15] M. A. Moiseev, *Radiophys. Quantum Electron.* **20**, 846 (1977).
  - [16] G. S. Nusinovich and H. Li, *Phys. Fluids B* **4**, 1058 (1992).
  - [17] P. E. Latham and G. S. Nusinovich, *Proc. SPIE* **2104**, 394 (1993).
  - [18] P. Malouff and V. L. Granatstein, *Int. J. Electron.* **72**, 943 (1992).
  - [19] W. Lawson *et al.*, *IEEE Trans. Plasma Sci.* **20**, 216 (1992).
  - [20] W. Lawson *et al.*, *Int. J. Electron.* **61**, 969 (1986).
  - [21] J. P. Calame and W. Lawson, *IEEE Trans. Electron. Dev.* **38**, 1538 (1991).
  - [22] W. B. Herrmannsfeldt, SLAC Report No. 226, 1979 (unpublished).
  - [23] L. R. Barnett *et al.*, *Phys. Rev. Lett.* **63**, 1062 (1989).
  - [24] J. Benford and J. Swegle, *High-Power Microwaves* (Artech House, Inc., Norwood, MA, 1992), pp. 29–37.
  - [25] W. Lawson and V. Specht, *IEEE Trans. Electron. Dev.* **40**, 1322 (1993).
  - [26] M. I. Petelin and W. Kasperek, *Int. J. Electron.* **71**, 871 (1991).

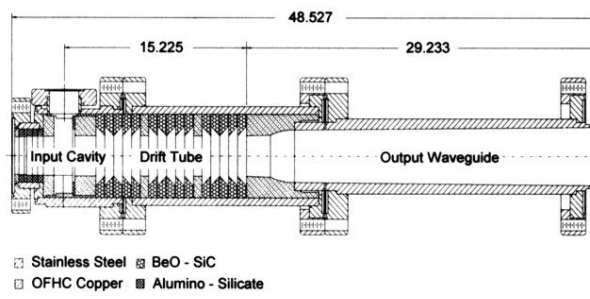


FIG. 1. Tube geometry. Dimensions indicated in cm.